

A numerical code for the solution of the Kompaneets equation in cosmological context

P. Procopio^{1,2} and C. Burigana^{1,2}

¹ INAF/IASF-BO, Istituto di Astrofisica Spaziale e Fisica Cosmica di Bologna, Via Gobetti 101, I-40129, Bologna, Italy

² Dipartimento di Fisica, Università degli Studi di Ferrara, Via Saragat 1, I-44100 Ferrara, Italy

Preprint online version: November 1, 2018

Abstract

Context. The cosmic microwave background (CMB) spectrum probes physical processes and astrophysical phenomena occurring at various epochs of the Universe evolution. Current and future CMB absolute temperature experiments are aimed to the discovery of the very small distortions such those associated to the cosmological reionization process or that could be generated by different kinds of earlier processes. The interpretation of future data calls for a continuous improvement in the theoretical modeling of CMB spectrum. **Aims.** In this work we describe the fundamental approach and, in particular, the update to recent NAG versions of a numerical code, KYPRIX, specifically written for the solution of the Kompaneets equation in cosmological context, first implemented in the years 1989-1991, aimed at the very accurate computation of the CMB spectral distortions under quite general assumptions. **Methods.** We describe the structure and the main subdivisions of the code and discuss the most relevant aspects of its technical implementation.

Results. We present some of fundamental tests we carried out to verify the accuracy, reliability, and performance of the code.

Conclusions. All the tests done demonstrates the reliability and versatility of the new code version and its very good accuracy and applicability to the scientific analysis of current CMB spectrum data and of much more precise measurements that will be available in the future. The recipes and tests described in this work can be also useful to implement accurate numerical codes for other scientific purposes using the same or similar numerical libraries or to verify the validity of different codes aimed at the same or similar problems.

Key words. Cosmic microwave background – Radiation mechanisms – Radiative transfer – Scattering

1. Introduction

The CMB spectrum emerges from the thermalization redshift, $z_{therm} \sim 10^6 - 10^7$, with a shape very close to a Planckian one, owing to the tight coupling between radiation and matter through Compton scattering and photon production/absorption processes, radiative Compton and bremsstrahlung. These processes were extremely efficient at early times and able to re-establish a blackbody (BB) spectrum from a perturbed one on timescales much shorter than the expansion time (see e.g. Danese & de Zotti (1977)). The value of z_{therm} (Burigana et al. 1991a) depends on the baryon density parameter, Ω_b , and the Hubble constant, H_0 , through the product $\widehat{\Omega} = \Omega_b(H_0/50)^2$ (H_0 expressed in Km/s/Mpc).

On the other hand, physical processes occurring at redshifts $z < z_{therm}$ may leave imprints on the CMB spectrum. Therefore, the CMB spectrum carries crucial informations on physical processes occurring during early cosmic epochs (see e.g. Danese & Burigana (1993) and references therein) and the comparison between models of CMB spectral distortions and CMB absolute temperature measures can constrain the physical parameters of the considered dissipation processes (Burigana et al. 1991a).

The timescale for the achievement of kinetic equilibrium between radiation and matter (i.e. the relaxation time for the photon spectrum), t_C , is

$$t_C = t_{\gamma e} \frac{m_e c^2}{k T_e} \simeq 4.5 \times 10^{28} (T_0/2.7 \text{ K})^{-1} \phi^{-1} \widehat{\Omega}^{-1} (1+z)^{-4} \text{ sec}, \quad (1)$$

where $t_{\gamma e} = 1/(n_e \sigma_T c)$ is the photon–electron collision time, $\phi = (T_e/T_r)$, T_e and $T_r = T_0(1+z)$ being respectively the electron and the CMB radiation temperature; $kT_e/m_e c^2$ (being m_e the electron mass) is the mean fractional change of photon energy in a scattering of cool photons off hot electrons, i.e. $T_e \gg T_r$; T_0 is the present radiation temperature related to the present radiation energy density by $\epsilon_{r0} = aT_0^4$ (here $a = 8\pi I_3 k^4/(hc)^3$, $I_3 = \pi^4/15$). A primordial helium abundance of 25% in mass is assumed in these numerical estimates. It is useful to introduce the dimensionless time variable $y_e(z)$ defined by

$$y_e(z) = \int_t^{t_0} \frac{dt}{t_C} = \int_1^{1+z} \frac{d(1+z) t_{exp}}{1+z} \quad (2)$$

where t is the time, t_0 is the present time, and $t_{exp} = 1/H = 1/[(da/dt)/a]$ is the expansion time, $a = 1/(1+z)$ being the cosmic scale factor normalized to the present time.

As particular cases, by neglecting the cosmological constant (or dark energy) contribution we have

$$t_{exp} \simeq 6.3 \times 10^{19} \left(\frac{T_0}{2.7 \text{ K}} \right)^{-2} (1+z)^{-3/2} \times \quad (3)$$

$$\left[\kappa(1+z) + (1+z_{eq}) - \left(\frac{\Omega_{nr} - 1}{\Omega_{nr}} \right) \left(\frac{1+z_{eq}}{1+z} \right) \right]^{-1/2} \text{ sec},$$

The address to which the proofs have to be sent is:
Carlo Burigana
INAF-IASF Bologna, Via Gobetti 101, I-40129, Bologna, Italy
fax: +39-051-6398724
e-mail: burigana@iasfbo.inaf.it

where $z_{eq} = 1.0 \times 10^4 (T_0/2.7 K)^{-4} \widehat{\Omega}_{nr}$ is the redshift of equal non relativistic matter and photon energy densities and $\kappa = 1 + N_\nu(7/8)(4/11)^{4/3}$, N_ν being the number of relativistic, 2–component, neutrino species (for 3 species of massless neutrinos, $\kappa \approx 1.68$), takes into account the contribution of relativistic neutrinos to the dynamics of the Universe¹, while assuming $\Omega_K = 0$, $\Omega_\Lambda = 1 - \Omega_{nr}$, and neglecting the radiation energy density, as possible at relatively low redshifts, we have

$$t_{exp} \simeq (1/H_0) [\Omega_{nr}(1+z)^3 + 1 - \Omega_{nr}]^{-1/2} \text{ sec}, \quad (4)$$

where $1/H_0 \simeq 3.1 \times 10^{17} h^{-1} \text{ sec}$ ($h = H_0/100$).

The time evolution of the photon occupation number, $\eta(\nu, t)$, under the combined effect of Compton scattering and of photon production processes, namely radiative Compton (RC) (Gould 1984), bremsstrahlung (B) (Karzas & Latter 1961; Rybicki & Lightman 1979), plus other possible photon emission/absorption contributions (EM)², is well described by the complete Kompaneets equation (Kompaneets 1956; Burigana et al. 1995):

$$\frac{\partial \eta}{\partial t} = \frac{1}{\phi} \frac{1}{t_c} \frac{1}{x^2} \frac{\partial}{\partial x} \left[x^4 \left[\phi \frac{\partial \eta}{\partial x} + \eta(1 + \eta) \right] \right] + \left[\frac{\partial \eta}{\partial t} \right]_{RC} + \left[\frac{\partial \eta}{\partial t} \right]_B + \left[\frac{\partial \eta}{\partial t} \right]_{EM}. \quad (5)$$

This equation is coupled to the time differential equation governing the electron temperature evolution for an arbitrary radiation spectrum in the presence of Compton scattering, energy losses due to radiative Compton and bremsstrahlung, adiabatic cooling, plus possible external heating sources, $q = a^{-3}(dQ/dt)$,

$$\frac{dT_e}{dt} = \frac{T_{eq,C} - T_e}{(27/28)t_{ey}} - \frac{2T_e}{t_{exp}} + \left[\frac{dT_e}{dt} \right]_{RC,B} + \frac{(32/27)q}{3n_e k}; \quad (6)$$

here $T_{eq,C} = [h \int \eta(1 + \eta)v^4 dv] / [4k \int \eta v^3 dv]$ is the Compton equilibrium electron temperature (Peyraud 1968; Zeldovich & Levich 1970), $t_{ey} = 3m_e c / 4\sigma_T \epsilon_r$, $\epsilon_r \simeq \epsilon_{r0}(1+z)^4$ being $\epsilon_{r0} = aT_0^4$ the radiation energy density today, and $x = h\nu_0/kT_0 = h\nu_0(1+z)/kT_0(1+z)$ is a dimensionless, redshift independent, frequency (ν_0 being the present frequency).

2. Setting up the problem

Partial differential linear equations are divided in three classes: elliptic, parabolic and hyperbolic. The Kompaneets equation is a parabolic partial differential equation (Tricomi 1957). Solutions to this equation under general conditions have to be searched

¹Strictly speaking the present ratio of neutrino to photon energy densities, and hence the value of κ , is itself a function of the amount of energy dissipated. The effect, however, is never very important and is negligible for very small distortions.

²A process that in principle should be included is the cyclotron emission. On the other hand, for realistic values of cosmic magnetic field, the cyclotron process never plays an important role for (global) CMB spectral distortions when ordinary and stimulated emission and absorption are properly taken into account and CMB realistic distorted spectra are considered (Zizzo & Burigana 2005). In fact, the cyclotron term may be significant, in the case of deviations of η from the BB distribution at the electron temperature, only at very long wavelengths, corresponding to the cyclotron frequency, where, during the formation of a spectral distortion, FF and RC are able to keep η extremely close to the BB equilibrium.

numerically, because it is impossible to find analytical solutions that accurately take into account the many kinds of cosmological scenarios and the great number of relevant physical processes. The numerical code KYPRIX was written to overcome the limited applicability of analytical solutions and to get a precise computation of the evolution of the photon distribution function for a wide range of cosmic epochs and for many cases of cosmological interest (Burigana et al. 1991a). KYPRIX makes use of the NAG libraries (NAG Ltd 2009).

Besides these libraries, a lot of numerical algorithms are used in the code: we used some of the routines available to the scientific community, but often we did write routines dedicated to a specific task. Among the formers, the D03PCF routine of the current version of the NAG release has been used to reduce the Kompaneets equation into a system of ordinary differential equations (Dew & Walsh 1981; Berzins et al. 1989; Berzins 1990; Skeel & Berzins 1990). The D03PGF routine used in the first versions of KYPRIX is no longer available (see also Sect. 3.2). The two codes work adopting the same numerical framework or, in other words, the D03PCF routine of the current NAG release corresponds to the D03PGF routine of the NAG release used in the first versions of KYPRIX. On the other hand, they come from different technical implementations and exhibit remarkable differences in several aspects. The main differences between the two routines, their usage, and the corresponding implications for the code KYPRIX will be described in this work. In order to use the D03PCF routine, we have to put the Kompaneets equation in the form

$$\sum_{j=1}^{NPDE} P_{i,j} \frac{\partial U_j}{\partial Y} + Q_i = X^{-m} \frac{\partial}{\partial X} (X^m R_i); \quad (7)$$

where Y is the time variable and X the spatial variable. Here $i = 1$ and $NPDE = 1$. $P_{i,j}, Q_i, R_i$ depend on $x, t, U, \partial U/\partial x$, the vector U is defined as immediately below. In our case, $P_{i,j} = 1$ and $m = 0$ (Cartesian coordinates). Note that $P_{i,j}, Q_i, R_i$ do not depend on $\partial U/\partial t$.

The variables that enter in this equation are introduced and used in logarithmic form, to have a good and essentially uniform accuracy of the solution in the whole considered frequency range. They are $X = \log(x)$ and $U = \log(\eta)$. Hereafter, we will use the variables X, U, Y for what concerns the informatic aspect of the problem, keeping the use of the variables x, η, y for considerations directly linked to physical aspects. The function R_i is determined only by the inverse Compton term while the other physical processes, i.e. at least Compton scattering, bremsstrahlung, and radiative Compton, are included in the function Q_i . In order to reduce Eq. (7) into a system of ordinary differential equations, the D03PCF routine uses the method of lines: the right member of Eq. (7) is discretized, reducing the calculation of partial derivatives in terms of finite values of the solution vector U at all the points of the X axis grid. Spatial discretization is made by the method of finite differences (Mitchell & Griffiths 1980). The resulting system of ordinary differential equations is solved using a differentiation formula method. The choice of the time parameter was driven by the need to have a very simple form of the Kompaneets equation. Finally, a ‘‘temperature independent’’ (time) Comptonization parameter

$$Y = y(t) = \int \frac{dy_e}{\phi} = \int_{t_i}^t n_e \sigma_T c \frac{kT_r}{mc^2} dt', \quad (8)$$

has found to be particularly advantageous (Burigana et al. 1991a).

2.1. Boundary conditions

Integrating equations of the type of Eq. (7) means to calculate the time evolution of the function $U(X, Y)$, for a given initial condition $U(X, 0)$ (in fact, the problem is also called “problem at initial conditions”). Numerically, the derivatives of U are replaced by finite differences between values of U computed at a grid of points (in X) and the differential equation is replaced by a system of more simple equations. However, in presence of the only initial condition, this system is singular (Press et al. 1992). For this reason, resolving partial differential parabolic equations needs boundary conditions: the problem is at initial values for the Y variable and at the boundary values for the X variable. In general, boundary conditions mean additional relations written to be joined to the system derived from the discretization to finite differences.

Therefore, a good statement of the problem needs the definition of appropriate boundary conditions. The capability of a refresh of these conditions along the integration in time leads more stability to the solution evolution because of the evolution of the radiation field. Thanks to the opportunity of having the correct value of ϕ for each time step, the update of the boundary conditions can be physically motivated (see also Sect. 3.2.6). The limits of the frequency range considered are: $X_{min} = \log(x_{min}) = -4.3$ e $X_{max} = \log(x_{max}) = 1.7$. Of course, we want a solution of the Kompaneets equation over all the frequency range where it is possible to measure the CMB. Also, we need to consider a frequency range large enough to contain, in practice, all the energy density of the cosmic radiation field.

The frequency range is so wide for the other two reasons described below.

During the time evolution, some spurious oscillations of the solution at points close to the boundaries may appear (these effects, that could also occur independently of the need of refreshing ϕ – for example for cases at constant ϕ –, may be partially amplified if, for computational reasons discussed in the following, the necessary refresh of the electronic temperature is not made for every time step). Fixing the frequency integration range limits far from the interval where we are interested to compute the photon distribution function allows to prevent the “contamination” of the solution by this possible spurious oscillations in the frequency range of interest.

Since we can generally assume that a Planckian spectrum at x_{min} is formed before recombination in a timescale shorter than the expansion time and, on the contrary, at x_{max} the shape of the spectrum is unknown, it has been implemented in the code the possibility to adopt a particular case of Neumann boundary conditions: the requirement that the current density, in the frequency space, is null at the boundaries of the integration range (Chang & Cooper 1970):

$$\left[\phi \frac{\partial \eta}{\partial x} + \eta(1 + \eta) \right]_{x=x_{min}, x_{max}} = 0. \quad (9)$$

This choice of boundary conditions formally satisfies the requirement of the problem when we integrate the Kompaneets equation in the case of Bose-Einstein like distortions (with a frequency dependent chemical potential, $\mu = \mu(x)$, vanishing at very low frequencies). In fact, such distorted spectra are indistinguishable from a blackbody spectrum at sufficiently high and at low frequencies.

Of course, it is possible to make a different choice of the boundary conditions by selecting Dirichlet like conditions. In this case the photon occupation number at the boundaries of

the integration interval does not change for the whole integration time. (In general cases, keeping constant conditions at the boundaries could be dangerous for the continuity of the solution. Nevertheless, for some specific problems this condition can work – typically for problems with constant ϕ).

3. A detailed view on KYPRIX

The code KYPRIX has been written to solve the Kompaneets equation in many kinds of situations. The physical processes that can be considered in KYPRIX are: Compton scattering, bremsstrahlung, radiative Compton scattering, sources of photons, energy injections without photon production, energy exchanges (heating or cooling processes) associated to $\phi \neq 1$ at low redshifts, radiative decays of massive particles, and so on (see e.g. Danese & Burigana (1993) for some applications). This code could be easily implemented to consider other kinds of physical processes. Various kinds of initial conditions for the problem can be considered and many of them have been already implemented in KYPRIX. The first obvious case is a pure Planckian spectrum. Several ways to model an instantaneous heating implying deviations from the Planckian spectrum have been introduced: a pure Bose-Einstein (BE) spectrum or a BE spectrum modified to become Planckian at low frequencies (this option could be exploited to integrate the Kompaneets equation with a constant ϕ and constant boundary conditions); a grey-body spectrum; a superposition of blackbodies.

The data are saved into five files.

DATI. This file contains the information about the specific parameters of the considered problem with a general description of its main aspects.

DATIP. In this file we give the evolution of interesting quantities, like time, redshift, ϕ , and another quantities inherent to physical and numerical aspects of the problem (see also Sect. 5.1).

DATIG. It contains: the grid of points for the X axis used by the main program (remember that we are using a dimensionless frequency), a Planckian spectrum at temperature T_0 and the solution vector U (that is to say $\log(\eta)$) at $y = 0$ (starting time).

DATIDE. This is the fundamental output file: it gives the solution of the Kompaneets equations at the desired cosmic epochs.

DATIT. It is similar to the file DATIDE, but it contains the solution in term of brightness temperature (i.e. equivalent thermodynamic temperature; see Eq. (12) in Sect. 3.2.2).

3.1. Main subdivisions

The code is divided in several sections and, from a general point of view, is structured as described here below.

1. Main program, in which many actions can be carried out: choice of the physical processes, choice of the cosmological parameters, initial conditions, characteristics of the numerical integration (accuracy, number of points of the grid), time interval of interest, choice of the boundary conditions, chemical abundances, ionization history.
2. Subroutine PDEDEF. It is the subprogram where the problem is numerically defined. This subroutine is also divided in subsections to allow modifications in a simple and practical way.
3. Subroutine BNDARY. Here the boundary conditions are numerically specified.
4. Subroutines and auxiliary functions to perform specific

calculations.

3.2. Technical specifications and code implementation

The first version³ of KYPRIX worked with the Mark 8 version of the NAG numerical library and were based on the routine D03PGF. The version of the NAG numerical library currently distributed is the Mark 21. Therefore an update of the code KYPRIX is necessary to adapt it to this new package.

When KYPRIX starts running it asks all the input data: from the declarations of the output files' names to the integration accuracy and features. In the following subsections we give a description of the various aspects of the code (and of its update), trying to give relevant hints about computational aspect of the code.

3.2.1. Grid

The frequency integration interval is divided in a grid of points (the mesh points): larger the number of points smaller the adopted frequency step. We adopted an equispaced grid in X . It is possible to use a very dense grid (for example 36001 mesh points corresponding to 36000 frequency steps). In general, it is necessary to use at least 3001 mesh points to have a solution accurate enough.

We found an important difference between the two NAG versions, not reported in the documentation of the routine D03PCF. In the first version (D03PGF), the subroutine where the partial differential equation is defined adopted the same mesh points defined in the main program. In the Mark 21 version the calculation is carried out in a different manner: the mesh points used in the subroutine PDEDEF is shifted of half spatial step with respect to the mesh defined in the main program. In this way, the mesh points in the PDEDEF subroutine will be exactly in the middle of the steps defined in the grid of the main program. For this reason, the limit of the integration interval are not considered in the mesh points in the subroutine PDEDEF and they are used only for the boundary conditions.

The effect of this feature implies the definition of new parameters that play a fundamental role in the subroutine PDEDEF. The integral quantities in the Kompaneets equation (necessary to define the radiative Compton term in the kinetic equations and the electron temperature) are computed once for any time step, inside the PDEDEF subroutine. For this computation, arrays of dimension equal to the number of mesh points of the x variable as defined in the PDEDEF subroutine are used. Therefore, a particular care must be taken in the definition of the dimension of the arrays defined in KYPRIX. Those used in the main program have dimension equal to the number of points of the mesh defined in the main program. The same dimension is given for the arrays defined for the boundary conditions. On the other hand, the major number of arrays are used in the PDEDEF subroutine to compute the integral quantities. The "inner" grid adopted in the PDEDEF subroutine is based on mesh points in the middle of the spatial steps of the main program grid, so the two grids can not work with the same point number; in fact, the arrays used in the PDEDEF subroutine have dimension $NPTS - 1$. Therefore, in the main program and in the subroutine BNDARY we have to work with arrays based on the formula:

$$X(I) = A + (I - 1) \times \frac{(B - A)}{(NPTS - 1)}, \quad (10)$$

with $1 \leq X \leq NPTS$,

to define the correspondence between the grid of $NPTS$ points and the X position, while we need another expression able to shift of half step the grid in the PDEDEF subroutine and based on $NPTS - 1$ mesh points:

$$X(I) = \left(A + (I - 1) \times \frac{(B - A)}{(NPTS - 1)} \right) + \left(\frac{(B - A)}{2(NPTS - 1)} \right), \quad (11)$$

with $1 \leq X \leq NPTS - 1$.

For continuity reasons, we need to define (according to the choices made in the main program) the solution vector, containing the photon initial distribution function, at the beginning of the integration also according to this grid definition. This vector is used by the PDEDEF subroutine as initial spectrum adopted for the computation of the rates of the physical processes and, of course, it is then renewed at every time step incrementation.

3.2.2. Output

Concerning the output files, the update version of KYPRIX stores a new vector containing the "inner" X grid used by the PDEDEF subroutine, XXGR (XGR refers to the main program X grid).

In addition, we preferred to have the possibility to perform the conversion of the solution into equivalent thermodynamic temperature directly into the code and save it in a new output file (DATIT). The conversion relation is:

$$T_{term,equiv} = \frac{xT_0}{\ln(1 + 1/\eta)} \quad (12)$$

(we remember that in the code $X = \log_{10}(x)$ and $U = \log_{10}(\eta)$). The fundamental reason to perform this conversion directly in the code is associated to the extreme accuracy required for the solution in the case of very small distortions, of particular interest given the FIRAS results (Fixsen et al. 1996). During the first tests, the conversion of the solution in brightness temperature was performed at the same time of the solution visualization, through the IDL visualization program. The saving of the solution into files is typically performed not for all the points of the grid but for a reduced grid of, for example, 300 equidistant points along the original grid to avoid to store files of large size, useless for our scope, given the interest for the CMB continuous spectrum (by definition, the Kompaneets equation is not appropriate to treat recombination lines). If the considered distortions were very small then the solution at each specific "inner" grid point could be affected by a numerical uncertainty not negligible in comparison with the very small deviations from a Planckian spectrum relevant in this cases. This numerical error is greatly reduced (becoming negligible for our purposes) by the averaging over a suitable number of grid points. Of course, the storing of the solution directly on a limited number of grid points makes this averaging no longer possible on the stored data. It were then necessary to average the solution values in intervals corresponding to the output x grid directly into the code. Anyway, in many circumstances the diagram shape derived applying the conversion to brightness temperature only on the stored averaged solution still deviates at high frequencies from the effectively computed solution displayed by considering all the "inner" grid points because of the high gradients in the photon distribution function and/or in the brightness temperature that makes difficult, or impossible, to find a general rule for the solution binning

³Written in 1989 by C. Burigana.

that simultaneously works properly for the two solution representations. This problem is avoided converting the solution vector in equivalent thermodynamic temperature before of the binning of its values and then applying the binning to the equivalent thermodynamic temperature. The result is then a brightness temperature diagram very clean and precise, even for very small distortions.

Other minor changes are made about the output data, where we passed from real to double precision, and for the saving frequency into the output files.

3.2.3. Equation formalism

A necessary update of the code has been performed to adapt it to the different formalism adopted by the new version of the NAG routine. This regards the expression of the Kompaneets equation in the PDEDEF subroutine. In particular, the D03PGF routine adopted the following expression of the partial differential equation:

$$C_i \frac{\partial U_i}{\partial Y} = X^{-m} \sum_{j=1}^{NPDE} \frac{\partial}{\partial X} \left[X^m G_{ij} \frac{\partial U_j}{\partial X} \right] + F_i, \quad (13)$$

where $i = 1, 2, \dots, NPDE$ (number of partial differential equations); C_i, F_i depends on $X, Y, U, \partial U / \partial X$; $G_{i,j}$ depends on X, Y, U and U is the set of solutions values ($U_1, U_2, \dots, U_{NPDE}$).

The expression now adopted by the D03PCF routine is represented by Eq. (7).

It is simple to translate the code from the old to the new formalism. In the considered case $NPDE = 1$. In this case, we have simply that R_1 contains both the function G_1 and the vector solution derivative with respect to X according to:

$$R_1 = G_{11} \times \frac{\partial U_1}{\partial X}. \quad (14)$$

At this point, it is necessary to apply only the following substitutions:

$$Q_1 = -F_1 \quad \text{and} \quad P_{11} = C_1. \quad (15)$$

With respect to this formalism, it is not difficult to adapt the various terms of the Kompaneets equation to the D03PCF routine. The terms that describe Radiative Compton, bremsstrahlung, (optional) electromagnetic processes and part of the contribution of the Compton scattering are counted in the function Q_1 . Instead, the second derivative of the solution vector with respect to X , which represents part of the inverse Compton rate, is counted in the function R_1 . So, according to these settings, we can write:

$$Q_1 = FC + FBREM + FRAD + FDEC, \quad (16)$$

where FC stands for the contribution of the Compton scattering, $FBREM$ the bremsstrahlung one, $FRAD$ the radiative Compton one and $FDEC$ represents the contribution of radiative decaying of particles. These terms are written in the form:

$$FC = \left[\phi \frac{\partial U}{\partial X} \left(\frac{\partial U}{\partial X} + 3 \right) + 10^X \left(\frac{\partial U}{\partial X} + 4 \right) + 2 \times 10^X 10^U \left(\frac{\partial U}{\partial X} + 2 \right) \right] \frac{1}{\ln(10)} \quad (17)$$

and

$$FBREM + FRAD = \frac{(e^{10^X})^\phi}{10^{3X}} \times \left\{ \frac{1}{10^U} - \left[(e^{10^X})^{\phi-1} - 1 \right] \right\} \times \left(FF0 \times W \times 1.5 \phi^{-1/5} \times FGAUNT + \frac{DC0}{W} I_1 \times GDC \right), \quad (18)$$

where $FF0$ and $DC0$ are the coefficients for the rates of bremsstrahlung and radiative Compton respectively; $FGAUNT$ and GDC represent the Gaunt factor corrections for bremsstrahlung and radiative Compton, respectively; I_1 is an integral quantity refreshed at every time step (see also Sect. 3.2.7).

The inverse Compton contributes to R_1 in this way:

$$R_1 = \frac{\partial U}{\partial X} \times \phi \times \ln(10)^{-2}. \quad (19)$$

Finally, we can put $P_{11} = 1$.

Furthermore, it is possible to add other source terms⁴ in Eq. (16).

3.2.4. Boundary conditions

Also notable are the differences between the input expressions defining the boundary conditions. The D03PGF routine adopted an expression of the form:

$$P_i(Y)U_i + Q_i(Y) \frac{\partial U_i}{\partial X} = R_i(Y, U), \quad (20)$$

where $i = 1, 2, \dots, NPDE$ and $P_i(Y), R_i(Y, U), Q_i(Y)$ are functions to be defined. A quite different notation is used to provide the boundary conditions in the D03PCF routine:

$$\beta_i(X, Y)R_i(X, Y, U, U_X) = \gamma_i(X, Y, U, U_X), \quad (21)$$

where $i = 1, 2, \dots, NPDE$ and $\beta_i(X, Y)R_i(X, Y, U, U_X)$ and $\gamma_i(X, Y, U, U_X)$ are functions to be defined ($U_X \equiv \partial U / \partial X$).

As a consequence of this notation, Neumann like boundary conditions can be now specified according to the expression:

$$\beta(1) = 1 \quad (22)$$

$$\gamma(1) = -XVA \times (10^{U(1)} + 1) \times \ln 10^{-2} \quad (23)$$

where XVA is the vector related to the X position computed in A and the dimension of both the equations corresponds to the differential equation number. Similar conditions are defined for the other extreme of the integration interval $[A, B]$.

3.2.5. Accuracy parameters

Another considerable difference between the two library versions regards the definition of the integration accuracy parameter. D03PGF used three parameters for monitoring the local error estimate in the time direction, supplying a good versatility. RELERR and ABSERR were respectively the quantity for the relative and absolute component to be used in the error test. The third parameter, INORM, was used to define the error test. If $E(i, j)$ is the estimated error for U_i (the vector solution) at the $j - th$ point of the X grid, then the error test was:

⁴For example, an already implemented subroutine models a term, called here $FDEC$, to be added in Eq. (16) which accounts for contributions of possible radiative decays of massive particles in the primordial Universe.

- INORM = 0 $\Rightarrow |E(i, j)| \leq \text{ABSERR} + \text{RELERR} \times |U(i, j)|$
- INORM = 1 $\Rightarrow |E(i, j)| \leq \text{ABSERR} + \text{RELERR} \times \max_y |U(i, j)|$
- INORM = 2 $\Rightarrow \|E(i, j)\| \leq \text{ABSERR} + \text{RELERR} \times \|U(i, j)\|$.

Instead, according to the new library version we have to define only one parameter ACC, a positive quantity that monitors the local error in the time integration. If $E(i, j)$ is defined as above, then the error test is:

$$|E(i, j)| = \text{ACC} \times (1 + |U(i, j)|). \quad (24)$$

Note that this is equivalent to the error test implemented in the D03PGF routine in the case INORM = 0 and ABSERR = RELERR (= ACC).

3.2.6. Electron temperature

During the numerical integration, some subprograms use the distribution function calculated at that time to compute ϕ . The integrals to be computed are those that we find in the expression for $\phi_{eq,C}$:

$$\phi_{eq,C} = \frac{T_e}{T_\gamma} = \frac{\int_0^\infty \eta(\eta + 1)x^4 dx}{4 \int_0^\infty \eta x^3 dx}. \quad (25)$$

In this calculation, the integration range is obviously the integration interval considered for the problem: $A \leq X \leq B$ (that, in terms of mesh ordering, corresponds to the range between 1 and $NPTS$ or $NPTS - 1$). For computing these integrals, all the points of the grid are used. The integration is based on the NAG D01GAF routine, suitable for tabulated functions. The update value of ϕ is also used in the boundary conditions.

In the previous version of the code KYPRIX, the computation of integral quantities were performed through a specific modification of the NAG package implemented by the KYPRIX code author that allowed to recover the whole vector solution at each time step in the subroutines (and in particular in PDEDEF), while the original package made only available in PDEDEF the solution separately at each grid point (being in fact the package originally designed for “pure” partial differential equation, without terms involving integrals of the solution). This modification, possible thanks to the availability of the NAG sources (and, in practice, thanks to the relative simplicity of the early library versions), permitted to update the integral quantities perfectly according to the “implicit” scheme adopted by the code for the integration in time. This is no longer feasible. Therefore, the update of the integral quantities must be now performed with a “backward” scheme, saving the solution at the previous time step in a proper vector and using it in the computation at the given time step. As well known, “backward” schemes are typically less stable than implicit schemes. And, in fact, we verified in some cases the difficulty of the D03PCF routine to work implementing the update of the quantities corresponding to the integral terms in the Kompaneets equation (and in particular of ϕ) for each time step. This were likely due to numerical instabilities.

We have then introduced a new integer control parameter into the code: STEPFI. It determines the frequency for the update the dimensionless electron temperature ϕ , relevant, of course, in the case we want to perform an integration with a variable ϕ . We have checked that updating the integral terms in the Kompaneets equation not at every time step, but after a suitable number of time steps does not affect the accuracy of the solution. This is due to the fact that the time increasing in the code is performed

with very small steps while the physical variation of ϕ occurs on longer timescales⁵.

See Sect. 5.2.2 for tests regarding the implications of this new implementation of the electron temperature evolution.

3.2.7. Radiative Compton

In the computation of the radiative Compton term there is an integral term, I_1 , given by the numerator of the right member of Eq. 25 (see Eq. (16) in Burigana et al. (1995)), so it is necessary to harmonize its update according to the parameter STEPFI discussed in the previous subsection. In fact, a possible asynchronous update of it and ϕ could create numerical instabilities and the crash of the code run, as physically evident from the great relevance of both radiative Compton term (at least at high redshifts) and electron temperature for the evolution of the low frequency region of the spectrum.

3.2.8. Integration routines

The global accuracy of the code KYPRIX depends on the accuracy of the solver for the partial differential equation as well as on the accuracy of all the other routines dedicated to different specific computations. In this section we focus on the routines of numerical integration used in the KYPRIX. As discussed in the previous subsections the D01GAF routine has been used for tabulated functions. On the other hand, KYPRIX involves the computation of integrals of various functions defined by analytical expressions, namely the parameters characterizing different types of initial conditions for the distorted spectra, as the amount of fractional injected energy and the electron temperature, and the relationship between the different time variables entering in the code (see also Sect. 4.1). Ultimately, the better accuracy in these specific computations implies a better global accuracy of KYPRIX. In the early release of the code KYPRIX the NAG D01BDF routine was used to calculate integrals of a function over a finite interval. The same task can be carried out by the D01AJF routine. This code offers a better accuracy than D01BDF (D01AJF is in fact suitable also to integrate functions with singularities, both algebraic and logarithmic). After the routines substitution, the results showed a great increasing of accuracy. In particular, this improvement offers the possibility to investigate also very small distortions that requires a very precise determination of all the relevant quantities because the absolute numerical error of the integration must be much smaller than the (very small quantities) of interest in these cases. In particular, the quantity $\Delta\epsilon_r/\epsilon_r$ (where ϵ_r is the actual density energy and ϵ_i is the energy density corresponding to the unperturbed distribution function just before the energy injection) must be constant during all the integration process in the absence of energy injection terms, according to the energy conservation. The precision increase on the computation of this quantity was noteworthy, keeping now always inside a few percent of the physical value (and its possible physical variation; see Sect. 5.1) of the same quantity independently of the magnitude of the considered distortion, allowing at the same time to accurately check the global accuracy of the code, improved thanks to the better computation of all the integral

⁵Of course, for physical processes with a stronger variation of the electron temperature, the accuracy parameter (see previous subsection) should be good enough to force the code to adopt sufficiently small time steps.

terms appearing in the Kompaneets equation. The remarkable improving in energy conservation even in the case of very small distortions is an important feature of the new version of KYPRIX that makes it applicable to a wider set of cases.

4. New physical options

4.1. Cosmological constant

About ten years ago, the relevance of the cosmological constant term (or of dark energy contribution) has been probed by a wide set of astronomical observations of type Ia Supernovae (Perlmutter et al. 1999; Riess et al. 1998). We have then updated the numerical integration code KYPRIX to include the cosmological constant in the terms controlling the general expansion of the Universe. In particular the input background cosmological parameters considered in the code are now: $T_0, \kappa, h [= H_0/(100\text{Km/s/Mpc})], \Omega_m, \Omega_b, \Omega_\Lambda, \Omega_K$, i.e. the present CMB temperature, the contribution of massless neutrinos, the Hubble constant, the (non relativistic) matter and baryon energy density, the energy densities corresponding to cosmological constant and curvature terms.

In order to compute the proper cosmic evolution of the various terms, an (increasing with time) scale factor parameter ω (Silk & Stebbins 1983), defined by

$$\omega = \frac{a}{a_1} \equiv \frac{m_e c^2}{kT_0} \frac{1}{1+z} = 1.98 \times 10^9 \Theta(1+z)^{-1}, \quad (26)$$

has been adopted (here $\Theta \equiv T_0/3^\circ\text{K}$ and the index 1 is referred to a particular epoch, when the CMB energy density was equal to the electron mass⁶: $kT(a_1) = m_e c^2$). To write a suitable expression for its time evolution we have to introduce two new key parameters

$$\beta = \frac{\rho_{m1}}{\rho_{r1}} = 3.5 \times 10^{-6} \frac{h^2}{\Theta^3} \Omega_{tot} \quad (27)$$

that is the initial ratio between matter energy density and radiation energy density, and

$$\frac{1}{\tau_{g1}} = \left(\frac{8\pi}{3} G \rho_{r1} \right)^{1/2} = \left[\frac{8\pi}{3} G \frac{a}{c^2} \left(\frac{m_e c^2}{k} \right)^4 \right]^{1/2} = 0.076 \text{s}^{-1} \quad (28)$$

defined as a initial gravitational time scale. The quantities with the index 1 refer to the epoch when $a = a_1$, with the index 0 when $t = t_0$ (today); ρ_{r1} and ρ_{m1} are related to ρ_r and ρ_m by

$$\rho_r = \rho_{0r} \left(\frac{\omega_0}{\omega} \right)^4 = \rho_{r1} \frac{1}{\omega^4}; \quad \rho_m = \rho_{0m} \left(\frac{\omega_0}{\omega} \right)^3 = \rho_{m1} \frac{1}{\omega^3}, \quad (29)$$

respectively.

Now we can define an equation for the evolution of ω :

$$\frac{\dot{\omega}}{\omega} = \left[\frac{8\pi}{3} G \rho(\omega) \right]^{1/2} = \quad (30)$$

$$\frac{8\pi}{3} G \left[\frac{\rho_{r1} K}{\omega^4} + \frac{\rho_{m1}}{\omega^3} + \frac{\rho_{K1}}{\omega^2} + \rho_\Lambda \right],$$

where we have included the contribution of massless relativistic neutrinos in the term κ (see also footnote 1; the term κ should be

⁶So, the parameter ω is analogous to the scale factor a , but normalized at the epoch in which $a = a_1$, that is to say when $kT = m_e c^2$.

properly evaluated considering also possible energy injections after neutrino decoupling).

After some calculations, we can finally write the completed and updated expression of $dt/d\omega$:

$$\frac{1}{\dot{\omega}} = \frac{\tau_{g1} \omega}{\left[1 + \beta \omega \left(1 + \frac{\Omega_{K/m} \omega}{2.164 \times 10^9} + \frac{\Omega_{\Lambda/m} \omega^3}{2.164 \times 10^{27}} \right) \right]^{1/2}}, \quad (31)$$

where $\Omega_{x/y} = \Omega_x/\Omega_y$.

The equation for $\dot{\omega}$ has to be inserted in the expression giving $dy = a_c dt$, which is inside the integral used to compute the time variable $y(\omega) = \int_{\omega_{start}}^{\omega} dy$ because we set $y = 0$ when the integration starts at $\omega = \omega_{start}$ (or equivalently at $z = z_{start}$). Finally, the expression for the time evolution of ω and y are related by the variable change:

$$dy = a_c dt = a_c \frac{dt}{d\omega} d\omega = a_c \frac{\omega}{\dot{\omega}} \frac{1}{\omega} d\omega, \quad (32)$$

where $a_c = \phi/(\tau_{c1} \omega^4)$ ($\tau_{c1} = 2.638 \times 10^{-9} \Theta^3/(h^2 \Omega_b)$).

The implementation of the cosmological constant and curvature terms makes the code KYPRIX suitable to be applied to interesting cases at late ages, including cosmic epochs at $z < 1$ when Λ supplies the greatest contribution to the expansion rate of the Universe. Remarkable examples are spectral distortions associated to the reionization of the Universe that, in typical astrophysical scenarios, starts at relatively low redshifts ($z \lesssim 10 - 20$). For sake of completeness, a few words about the computation of the time evolution in the code. The subroutine called WDIY0 is the core of the time evolution in KYPRIX: it computes the value of ω given a value of y . This process takes advantages of the definition of y as integral of dy and, of course, it happens at each time step. To do this, we make use of a double precision version of the function ZBRENT, from ‘‘Numerical Recipes’’ (Press et al. 1992).

4.2. Chemical abundances

In this new version of the code it is possible to choose the primordial abundances of H and He . We have consistently computed the electron number density, n_e , involved in the different physical processes. In the previous implementation it was assumed a fixed abundance of H and He (and full ionization). The electron number density was then given by

$$n_e^{free} = n_e^{tot} \simeq \frac{\rho_b}{m_b} \frac{7}{8}, \quad (33)$$

where ρ_b is the baryon density and m_b the mean mass of a baryon. Now, denoting with f_H the fraction in mass of primordial H and considering that $n_e = n_H + 2n_{He}$, we have

$$n_e^{free} = n_e^{tot} = \frac{1 + f_H}{2} \frac{\rho_b}{m_b}. \quad (34)$$

This obviously impacts the physical processes involved in the code. Note that Compton scattering, radiative Compton, and bremsstrahlung depend linearly⁷ on n_e^{free} .

⁷For bremsstrahlung, the dependence on the densities of nuclei is now explicit.

4.3. Ionization history

In the last years, CMB observations are getting a very high accuracy, in particular regarding the angular power spectrum of temperature anisotropies albeit also for that of E mode polarization and cross-correlation (see e.g. Nolta et al. (2009)). A detailed understanding of the cosmological reionization process is crucial for precisely modeling the power spectrum of CMB anisotropies in comparison with current data, while a better treatment of recombination is of great relevance in the view of the data expected by the forthcoming ESA *Planck* satellite⁸ (The Planck Collaboration 2006).

An accurate modeling of the ionization history is crucial also for the precise computation of CMB spectral distortions in the view of the comparison with data from a future generation of high sensitivity experiments. We have then included these aspects in the current implementation of KYPRIX. In particular, the fraction of each state of ionization of the relevant elements (hydrogen, H , and helium, He) has been implemented.

The effects of this implementation is negligible⁹ in practice for the radiative Compton, because during the epochs this process is active the medium is fully ionized. Instead, Compton scattering and bremsstrahlung rates are significantly influenced by this implementation.

Once introduced the electron ionization fraction in the code, χ_e , which gives the number of electrons that takes part in the physical processes, we can choose different ways by which the active fractions of elements can play their roles in the phenomena.

Given χ_e , from the charge conservation law we have a constraint on the number of the free ions in the considered plasma. The simplest way to take count of them in the code is to assume an equal fraction of ionization for H and He . Of course, this is a toy model, but this parametrization was very useful to test the code.

A somewhat more accurate treatment of the physics of reionization/recombination processes implemented in the code is based on the Saha equation:

$$\frac{n_{i+1}n_e}{n_i} = \frac{2}{\Lambda^3} \frac{g_{i+1}}{g_i} e^{-\frac{\epsilon_{i+1}-\epsilon_i}{k_B T}}, \quad (35)$$

where n_i is the density of atoms in the i -th state of ionization, n_e is the electron density, g_i is the degeneracy of states for the i -ions, ϵ_i is the energy required to remove i electrons from a neutral atom and Λ is the thermal de Broglie wavelength of an electron, defined by

$$\Lambda = \sqrt{\frac{h^2}{2\pi m_e k_B T}}. \quad (36)$$

Providing the electron ionization fraction defined as¹⁰

$$\chi_e \equiv \frac{n_e^{free}}{n_e^{tot}}, \quad (37)$$

we can compute the unknowns $\chi_H, \chi_{H^+}, \chi_{He}, \chi_{He^+}, \chi_{He^{++}}$, defined as the relative abundances of the different ionization states of each element with respect to the global number density of the element. The Saha equation provides the ratio between two state of ionization of a single specie, once given the electron density and the temperature:

$$\frac{n_{H^+}}{n_H}, \frac{n_{He^+}}{n_{He}}, \frac{n_{He^{++}}}{n_{He^+}}. \quad (38)$$

To recover all the unknowns we need other relations. These additional conditions are provided by the charge conservation and the nuclei conservation.

From charge conservation it is possible to recover the contribution of the electrons related to a single specie to the total number of free electrons. The latter is of course related to the ionization fraction of all the involved species and can be written as:

$$n_e^{free} = \frac{\rho_b}{m_b} \left[\chi_{H^+} f_H + 2 \left(\frac{1-f_H}{4} \right) (\chi_{He^+} + \chi_{He^{++}}) \right], \quad (39)$$

where f_H is the fraction of primordial H described in the previous section. In Eq. (39) it is possible to identify the number of electrons coming from H and from He .

The nuclei conservation law separately for H and He is expressed by

$$n_H^{tot} = \frac{\rho_b}{m_b} [f_H (\chi_H + \chi_{H^+})], \quad (40)$$

$$n_{He}^{tot} = \frac{\rho_b}{m_b} \left[\left(\frac{1-f_H}{4} \right) (\chi_{He} + \chi_{He^+} + \chi_{He^{++}}) \right]. \quad (41)$$

Providing the electron ionization fraction and the temperature, it is possible to build two separate systems (one for H and one for He) in order to recover the considered ionization fractions.

The code can ingest a table with the desired evolution of χ_e and, as necessary for a physical modeling of cosmological reionization, of the electron temperature.

Obviously, we have implemented the best way to perform the exact calculation of the rates of considered processes in scenarios involving reionization/recombination which is that of using a co-running code, coupled to KYPRIX, able to supply the ionization fraction for all the species. For the recombination process, we developed an interface that allows the code to call an external program, in our case RECFAST (Seager et al. 1999), and run it with the same cosmological parameters selected for KYPRIX. Then KYPRIX will read the output table from RECFAST and will use the ionization fractions for the calculation of the rates of the processes, allowing a more detailed estimation of the spectral distortion arising during the recombination process (Wong et al. 2008). If we are interested in standard recombination, we adopt the equilibrium electron temperature (Eq. 25).

A consistent modeling of a modified recombination should provide the evolution of both electron temperature and ionization fractions (at least χ_e).

5. Tests on code performance, reliability, and accuracy

Once terminated the updating of the numeric integration code, we have carried out many accuracy and performance tests. Obviously, we have checked the physical meaning of the numerical solutions provided by the code comparing them with the

⁸<http://www.rssd.esa.int/planck>

⁹For example, for $z \lesssim 10^{-4}$ and $\Delta\epsilon_i/\epsilon_i = 10^{-5}$ we find that, for both BE and Comptonization like distortions, the rate of radiative Compton is less than 1/1000 of the rate of bremsstrahlung at each frequency of the grid.

¹⁰It is common to find in the literature χ_e normalized to the H number density. Obviously, the code can switch between the two conventions.

existing analytical solutions that in some cases can be considered as good approximations of exact solutions. In general, a code of good quality must have high numerical precision compared to the knowledge, both theoretical and observational, of the considered problem. Note also that various routines, mainly from the NAG package albeit also from the “Numerical Recipes” (Press et al. 1992) package, are used here for several specific computations. Since different routines can solve the same mathematical problems using different numerical methods and/or implementations with different settings and input parameters, we have verified that the adopted routines allow the appropriate accuracy and efficiency.

In the following subsections we will report on some specific quality tests of the numerical solutions. We comment now briefly on the code computational time.

In order to evaluate the global CPU time of the code we performed many runs with very different settings. These times are carried out testing the code on a machine with 4 Alpha CPUs, but effectively using only one CPU (now we are running the code on IBM Power5 Processors). The code global CPU time ranges from few minutes, for cases in which the integration starts at low redshifts, to about 5 hours, for some cases starting at very high redshifts ($y(z) \approx 5$). There are many variables that take role in determining the global CPU time. The complete Kompaneets equation involves in fact several terms. In the code KYPRIX we can select the physical processes to be considered in the numerical integration and the global CPU time increases with the number of activated processes.

Of course, the global CPU time depends on the parameters related to the numerical integration characteristics. The number of points adopted for the X grid (see Sect. 3.2.1) has a great influence on the global CPU time. Clearly, the integration accuracy improves with $NPTS$ and in many cases of interest it must be set to a very large value. We find that the global CPU time is approximately proportional to $NPTS$ ($t_{CPU} \propto NPTS$).

The parameter that plays the most relevant role in determining the global CPU time is the accuracy required for the time integration. The final solution precision depends on the value of the corresponding parameter ACC . Only for very high accuracy ($ACC \lesssim 10^{-12} - 10^{-14}$) the CPU time reaches the duration of some hours while keeping $ACC \sim 10^{-5}$ the integration is carried out in few minutes. Anyway, the limits imposed by CMB spectrum observations drive us to investigate in particular on small distortions. It is then necessary to work with low values of ACC (in general, $\lesssim 10^{-8}$).

After the assessment of the better choice for the use of the parameters of the various numerical routines and the definition of the accuracy of the integration in time, we have carried out several tests in order to verify the physical validity of the code results.

5.1. Energy conservation

In the code output file DATIP we store values of several parameters of interest. Two of them provide very useful information on the goodness of the numerical integration. The first one is the ratio, ϵ_r/ϵ_i , between the radiation energy density at each time and the energy density corresponding to the unperturbed distribution function before the distortion¹¹ in the absence of dissipa-

¹¹For example, for a Bose-Einstein distorted spectrum with a dimensionless chemical potential μ_0 produced by an energy dissipation with negligible photon production $\epsilon_r/\epsilon_i = f(\mu_0)/\varphi^{4/3}(\mu_0)$ (see e.g.

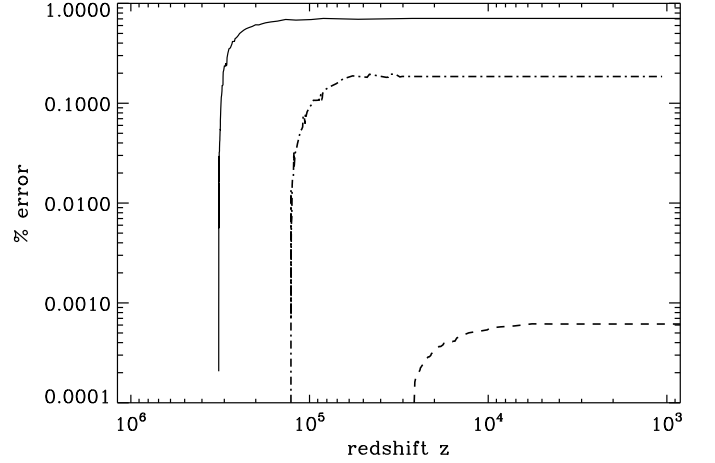


Figure 1. Error in the energy conservation expressed in terms of relative (%) deviation from its input value of the quantity $\Delta\epsilon_r/\epsilon_i = 10^{-5}$. The accuracy of the integration in time is set to $ACC = 10^{-12}$ (see also the text for further details on computation). Solid, dot-dashed, and dashed lines refer to an energy injection occurred respectively at $y_h(z) \approx 1.5, 0.25, 0.01$. Obviously, this error further decreases improving the accuracy parameter adopted in the numerical integration.

tion processes, the exact energy conservation is represented by the constance of this ratio during the integration. To quantify the accuracy supplied by KYPRIX, the values of ϵ_r/ϵ_i are stored at the starting of the integration and at many following times. In order to estimate the precision of the energy conservation, we define the quantity:

$$ERR_\epsilon = \frac{|(\epsilon_r/\epsilon_i)_{t=t_{start}} - (\epsilon_r/\epsilon_i)_{t>t_{start}}|}{(\epsilon_r/\epsilon_i)_{t=t_{start}} - 1}, \quad (42)$$

that gives the relative induced error in the energy conservation with respect to the initial value of $\Delta\epsilon_r/\epsilon_i$ or, more formally, the relative error induced by numerical uncertainty on the amount of fractional injected energy. Typical results obtained starting from a superposition of blackbodies are reported in Fig. 1.

Since the same absolute numerical integration error corresponds to a larger relative error for a smaller distortion, i.e. for smaller $\Delta\epsilon_r/\epsilon_i$ in these models, we could in principle expect a relative degradation of the energy conservation for decreasing distortion amplitudes. Our tests indicate in fact an increasing of the relative degradation of the energy conservation for decreasing distortions when the same accuracy parameters are adopted. On the other hand, one can select them according the specific problem. For example, considering an energy injection of $\Delta\epsilon_r/\epsilon_i = 10^{-5}$ occurred at $z \sim few \times 10^4$, an accuracy equal to $ACC = 10^{-8}$ is fully satisfactory for a very precise calculation of the photon distribution function, while for earlier processes, as for $z \gtrsim few \times 10^5$, and for the same injected fractional energy, the accuracy parameter needs to be set to $ACC \leq 10^{-12}$ in order to assure a calculation with ERR_ϵ less than 1%. Anyway, we find that for suitable choices of the integration accuracy parameters, ERR_ϵ can be kept always below $\approx 0.05\%$ without requiring a too

Sunyaev & Zeldovich (1970), Danese & de Zotti (1977) and also equations (8) and (9) in Burigana et al. (1991a) for the definition of $f(\mu_0)$ and $\varphi(\mu_0)$ for arbitrary values of μ_0 ; for $\mu_0 \ll 1$, $f(\mu_0) \approx 1 - 1.11\mu_0$ and $\varphi(\mu_0) \approx 1 - 1.368\mu_0$).

large computational time. Finally, we note that in some circumstances the scheme for the electron temperature evolution in the new version of KYPRIX (backward differences), different from that used in the original one (implicit scheme), could imply some small discontinuities in the evolution of the electron temperature and of $\Delta\epsilon_r/\epsilon_i$. On the other hand, we have verified that this effect does not affect the very good accuracy of the solution, because of the very small amplitude of these discontinuities (together with their localization to a very limited number of time steps) and of the corresponding energy conservation violation.

5.2. Comparative tests

5.2.1. Comparing solutions

The first kind of test is simple comparison between the results obtained with the update version of KYPRIX and those obtained with the original version for the same set of input parameters.

To this purpose, we have considered some interesting cases carried out in the past. In particular we used the input parameters adopted in (Burigana et al. 1995) where also semi-analytical descriptions of the numerical solutions of the Kompaneets equation were reported. We report here cases characterized by an amount of exchanged fractional energy $\Delta\epsilon_r/\epsilon_i = 10^{-4}$. We started the integration from a redshift corresponding to $y_h(z) \approx 0.25$ in one case and to $y_h(z) \approx 0.01$ for another. The input cosmological parameters are: $H_0 = 50$, $\bar{\Omega}_b = 0.03$, $k = 1.68$, $T_0 = 2.726$ K. The results given by the update version of KYPRIX (see Fig. 2) are fully consistent with those reported in Burigana et al. (1995). Moreover, since that paper provided also a seminanalytical description of the solution of the Kompaneets equation, it is clear that a good agreement of the numerical results obtained with the original and update code represents a further confirmation of the validity of the analytical description.

5.2.2. Electron temperature behavior

While the energy exchange between matter and radiation is leaded by Compton scattering (in the absence of external energy dissipation processes), electrons reach the equilibrium Compton temperature (Peyraud 1968; Zeldovich & Levich 1970), $T_{e,eq}$, in a time shorter than the expansion time. For $y_h \ll 1$, (late heating processes) Compton scattering is no longer able to significantly modify the shape of the perturbed spectrum and the final electronic temperature ϕ_f (remember that $\phi = T_e/T_r$), immediately after the decoupling, is very close to $\phi_{eq} = T_{e,eq}/T_r$. On the other hand, for energy injections at redshifts corresponding to $y_h \gtrsim 5$, Compton scattering can establish kinetic equilibrium between matter and radiation. This corresponds to a Bose-Einstein spectrum, with a final electron temperature given by (Sunyaev & Zeldovich 1970; Danese & de Zotti 1977):

$$\phi_f(y_h \gtrsim 5) = \phi_{BE} \approx (1 - 1.11\mu_0)^{-1/4}, \quad (43)$$

where $\mu_0 (\ll 1)$ is the usual dimensionless chemical potential. Moreover, in this case the evolution of the chemical potential, $\mu(z)$, the relation between it and the amount of fractional energy injected, $\Delta\epsilon/\epsilon_i$, depends on the energy injection epoch.

For the intermediate energy injection epochs, corresponding to $y_h \lesssim 5$, the final value of ϕ (a function depending on y_h) is between the values of ϕ_{BE} and ϕ_{eq} , because the Compton scattering works to produce a Bose-Einstein like spectrum anyway (Burigana et al. 1991a). At these epochs the relation between

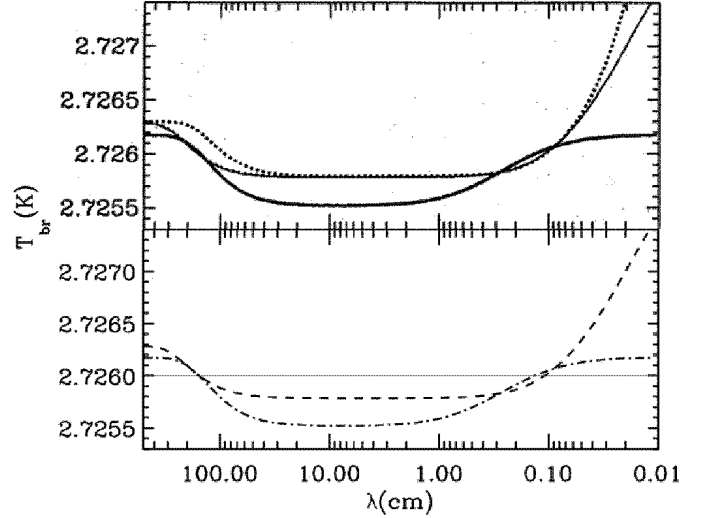


Figure 2. Comparison between the present time solution for the CMB spectrum obtained from the old version of the numerical code (top panel; adapted from panel a of Fig. 1 in Burigana et al. (1995)) and the current one (bottom panel). See the text for further details on computation parameters. Dashed (dot-dashed) line refers to an energy injection occurred at $y_h(z) \approx 0.01$ ($y_h(z) \approx 0.25$). Note the excellent agreement between the results of the two codes. In the case of the old version of the code we report also the analytical approximation (dotted line) described by a Comptonization spectrum plus a free-free distortion (see Eq. 50).

the chemical potential and the amount of fractional injected energy injected is simply given by (Sunyaev & Zeldovich 1970; Danese & de Zotti 1977):

$$\mu_0 \approx 1.4 \frac{\Delta\epsilon}{\epsilon_i}. \quad (44)$$

By exploiting the numerical results, a simple formula for ϕ can be found (Burigana et al. 1995):

$$\phi_f(y_h) = \frac{k}{5} \frac{5 - y_h}{k + y_h} (\phi_{eq} - \phi_{BE}) + \phi_{BE}; \quad (45)$$

here $k = 0.146$ is a constant derived from the fit. Moreover, this expression represents an accurate description of the evolution of ϕ for any value of y_h . In facts, for a value of y ($y < y_h$) they found:

$$\phi(y, y_h) = \phi_f(y_h - y). \quad (46)$$

In the considered cases, as in many situations of interest, the perturbed spectrum of the radiation (immediately after the heating process) is described by a superposition of blackbodies and the equilibrium temperature is given by (Zeldovich & Sunyaev 1969; Zeldovich et al. 1972; Burigana et al. 1995):

$$\phi_{eq} \approx (1 + 5.4u)\phi_i, \quad (47)$$

where $\phi_i = T_i/T_r = (1 + \Delta\epsilon/\epsilon_i)^{-1/4} \approx 1 - u$ and the Comptonization parameter u could be related to the amount of fractional energy exchanged by (Zeldovich & Sunyaev 1969; Zeldovich et al. 1972; Burigana et al. 1995):

$$u \approx (1/4)\Delta\epsilon/\epsilon_i. \quad (48)$$

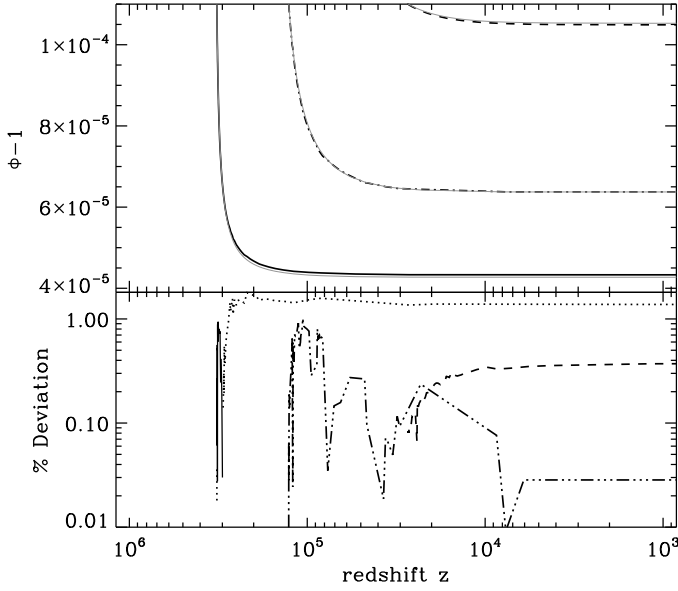


Figure 3. Top panel: evolution of ϕ as derived from the numerical code. The parameters adopted for the computation are the same as in Fig. 1 as well as the adopted kinds of lines. We report also for comparison the analytical results obtained from Eq. (45) (thin solid lines). Bottom panel: relative differences between the analytical results and the numerical results expressed in terms of $(\phi_{\text{analytical}} - \phi_{\text{numerical}})/(\phi_{\text{numerical}} - 1)$. Note that in absolute value they are $\leq 1\%$ at each time. Again, the adopted kinds of lines are as in Fig. 1, but solid line is replaced by dots when the above relative difference is negative.

Eqs. (45) and (46) can be used to test the behavior of the electron temperature during the numerical integration of the Kompaneets equation carried out with the new code version. With the increasing of the time variable, the values of ϕ are saved into the file DATIP, from the initial time step to the final one. The upper panel of Fig. 3 shows the two behaviors of ϕ (the numerical one and the analytical expression given by Eqs. (45) and (46)) while the bottom panel displays their relative difference.

This test is of particular importance for the check of the validity of the results because of the crucial role of ϕ in the Kompaneets equation. As remembered in the previous section, in the new version of the code a different scheme is used with respect to that implemented in the original version. The verification of the very good agreement of the above behaviors of ϕ further supports the substantial equivalence of the two code versions and their reliability. In particular, it confirms that the new adopted numerical scheme for the evolution of ϕ , in principle less stable than the implicit scheme implemented in the code original version, does not affect the validity of the solution.

5.3. Free-free distortion

As already discussed by Sunyaev & Zeldovich (1970), accurate measures of the CMB spectrum in the Rayleigh-Jeans region could provide quantitative informations about the thermal history of the Universe at primordial cosmic epochs. On the other hand, photon production processes (mainly radiative Compton at earlier epochs and bremsstrahlung at later epochs) work to reduce the CMB spectrum depression at long wavelengths (see Danese & de Zotti (1980)) since they try to establish a true

(Planckian) equilibrium. For $z < z_p$ (Danese & de Zotti 1980; Burigana et al. 1991a) with

$$z_p \approx 2.14 \times 10^4 \left(\frac{T_0}{2.7 \text{ K}} \right)^{1/2} \left(\frac{k}{1.68} \right)^{1/4} \widehat{\Omega}_b^{-1/2}, \quad (49)$$

low frequency photons are absorbed before Compton scattering moves them to higher frequencies.

In case of small and late distortions ($z_h \lesssim z_p$), a quite good approximation of the whole spectrum is given by (Burigana et al. 1995)

$$\eta(x, \tau) = \eta_i e^{-(\tau - \tau_h)} + e^{-(\tau - \tau_h)} \int_{\tau_h}^{\tau} e^{(\tau' - \tau_h)} \frac{1}{e^{x/\phi(\tau')} - 1} d\tau' + u \frac{x/\phi_i e^{x/\phi_i}}{(e^{x/\phi_i} - 1)^2} \left(\frac{x/\phi_i}{\tanh(x/2\phi_i)} - 4 \right), \quad (50)$$

where the index i denotes the initial value of the corresponding quantity and u is the Comptonization parameter. This expression provides also an exhaustive description of continuum spectral distortion generated in various scenarios of (standard or late) recombination or associated to the cosmological reionization. For an initial blackbody spectrum, at dimensionless frequencies $x_B \ll x \ll 1$ the above equation can be simplified to (Burigana et al. 1995)

$$\eta \approx \eta_{BB,i} + \frac{y_B}{x^3} - u \frac{2}{x/\phi_i}; \quad (51)$$

here y_B , an optical depth of the Universe for bremsstrahlung absorption (radiative Compton can be neglected at late epochs), is analogous to the Comptonization parameter and it is given by

$$y_B = \int_{t_h}^t (\phi - \phi_i) \phi^{-3/2} g_B(x, \phi) K_{0B} dt = \int_{1+z}^{1+z_h} (\phi - \phi_i) \phi^{-3/2} g_B(x, \phi) K_{0B} t_{exp} \frac{d(1+z)}{1+z}; \quad (52)$$

x_B is the frequency at which $y_{abs,B} = 1$ (Zeldovich et al. 1972; de Zotti 1986). The dependence of the Gaunt factor (Karzas & Latter 1961; Rybicki & Lightman 1979; Burigana et al. 1991a) on x and ϕ at very long wavelengths is weak: $g_B \propto \ln(x/\phi)$.

In terms of brightness temperature, the distortions at low frequencies (at any redshift) can be written as

$$\frac{T_{br} - T_r \phi_i}{T_r} \approx \frac{y_B}{x^2} - 2u \phi_i, \quad (53)$$

where $T_r = T_0(1+z)$. This approximation holds at low frequencies but not at too low frequencies, where the brightness temperature obviously approaches the electron temperature because of the extremely high efficiency of bremsstrahlung, still able to generate a Planckian spectrum at electron temperature.

In order to show that our numerical solution follows the behavior described by the above equation, we can compute y_B from the brightness temperature derived from the numerical solution:

$$y_B \approx x^2 \left(\frac{T_{br} - T_r \phi_i}{T_r} + 2u \phi_i \right). \quad (54)$$

The reported numerical result (see Fig. 4) refers to a heating process corresponding to a full reionization starting at $z \approx 20$ with $\phi = 10 \times 10^4$ K, producing a final Comptonization parameter $u \approx 4 \times 10^{-6}$ compatible with FIRAS upper limits. As shown

in Fig. 4, at low frequencies y_B approaches an almost constant value. This is correct only for $\lambda > 200 - 300$ cm while at higher frequencies y_B is no longer almost constant (see again Fig. 4) because of the dependence of the Gaunt factor on x and ϕ as expressed in the definition of y_B . We can also write an expression describing the brightness temperature through a constant parameter \bar{y}_B , derived from Eq. (54) (see Fig. 4) averaged over the range at very long frequencies before the y_B declining shown in Fig. 4, to verify the accuracy of the below expression

$$T_{br,y_B} = \left(\frac{\bar{y}_B}{x^2} - 2u\phi_i + \phi_i \right) \cdot T_r \quad (55)$$

in comparison with the numerical results. Note that where the Gaunt factor dependence on x and ϕ produces a significantly varying y_B (see Fig. 4), the Comptonization decrement is more relevant than the free-free excess in determining the brightness temperature, as evident from the good agreement of the two curves in Fig. 4. Clearly, the brightness temperature derived in this way works only up to frequencies (~ 100 GHz) approaching that at which the excess in the brightness temperature produced by the Comptonization begins (at ~ 220 GHz, see Fig. 4).

Note also that the use of \bar{y}_B in Eq. (55) implies a slight excess ($\sim (y_B - \bar{y}_B)T_r/x^2$) with respect to the accurate numerical results since y_B decreases with the frequency (see Fig. 4). In this representative test the excess is ≈ 0.1 mK, but obviously its value depends on the amplitude of free-free distortion (other than on the frequency). This error is clearly negligible for the analysis of current data (see e.g. Salvaterra & Burigana (2002a,b); Zannoni et al. (2008); Singal et al. (2009)). It is likely not so relevant for the analysis of future measures at $\lambda \gtrsim 1$ cm with accuracy comparable to that proposed for DIMES (Kogut 1996; Burigana & Salvaterra 2003). On the contrary, it could be relevant for a very accurate analysis of future measures at with precision comparable to that proposed for FIRAS II $\lambda \lesssim 1$ cm (Fixsen & Mather 2002; Burigana et al. 2004; Mather 2009) or thought in ideas for possible future long wavelength experiments from the Moon^{12,13} (Burigana et al. 2007). This calls for a complete frequency and thermal history dependent treatment of the free-free distortion in the accurate analysis of future data of extreme accuracy.

6. Discussion and conclusion

We have described the fundamental numerical approach and, in particular, the recent update to recent NAG versions of a numerical code, KYPRIX, specifically written for the solution of the Kompaneets equation in cosmological context, aimed to the very accurate computation of the CMB spectral distortions under quite general assumptions. The recipes and tests described in this work can be useful to implement accurate numerical codes for other scientific purposes using the same or similar numerical libraries or to verify the validity of different codes aimed at the same or similar problems.

Specifically, we have discussed the main subdivisions of the code and the most relevant aspects about technical specifications and code implementation. After a presentation of the equation formalism and of the boundary conditions added to the set of ordinary differential equations derived from the original parabolic partial differential equation, we have given details on the adopted space (i.e. dimensionless frequency) grid, on the output results,

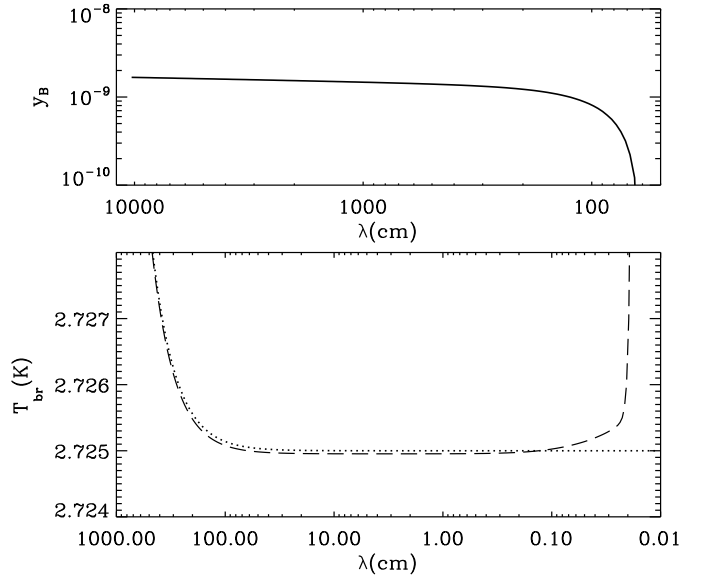


Figure 4. Top panel: y_B as derived from Eq. (54). Bottom panel: comparison between the numerical (long dashes) solution and the analytical approximation represented by Eq. (55). See the text for further details.

on the accuracy parameters, and on the used integration routines. The introduction of the time dependence of the ratio between electron and photon temperatures and of the radiative Compton scattering term, both introducing integral terms in the Kompaneets equation, has been addressed in the specific context of the recent NAG versions by discussing the solution adopted to solve the various related technical problems.

Some of the tests we carried out to verify the reliability, accuracy, and performance of the code are presented.

We have compared the results of the update version of the code with those obtained with the original one, reporting some representative cases, and we have found an excellent agreement.

Some specific quantitative tests are here reported. They indicate a very good accuracy in the energy conservation: for appropriate choices of the code accuracy parameters, the fractional injected energy is conserved within an accuracy better than 0.05%, or, in other words, possible energy conservation violations are negligible in practice for theoretical predictions and for comparison with current and future data. The time behavior of the electron temperature is found to be in excellent agreement with the results obtained with the original code version, in spite of the different schemes adopted to update the evolving electron temperature. These are important verifications that probe that the current implementation of the code KYPRIX circumvents the problem represented by the lost possibility of internally adapting the solver of partial differential equation to make it directly able to include integrals of the solution vector exactly at the current time step. Also, the setting of the accuracy parameters of the solver is now less flexible. Of course, these features imply a certain increase of complexity in the code implementation, usage, and in the setting of code parameters. In spite of these difficulties, thanks to the better treatment of various computational steps involving integrals of functions over finite intervals, the new version of KYPRIX achieves a good accuracy even in the treatment of very small distortions.

We have described also the introduction of the cosmological constant in the terms controlling the general expansion of the

¹²<http://www.lnf.infn.it/conference/moon07/Program.html>

¹³<http://sci.esa.int/science-e/www/object/index.cfm?fobjectid=40925>

Universe in agreement with the current concordance model, of the relevant chemical abundances, and on the ionization history, from recombination to cosmological reionization.

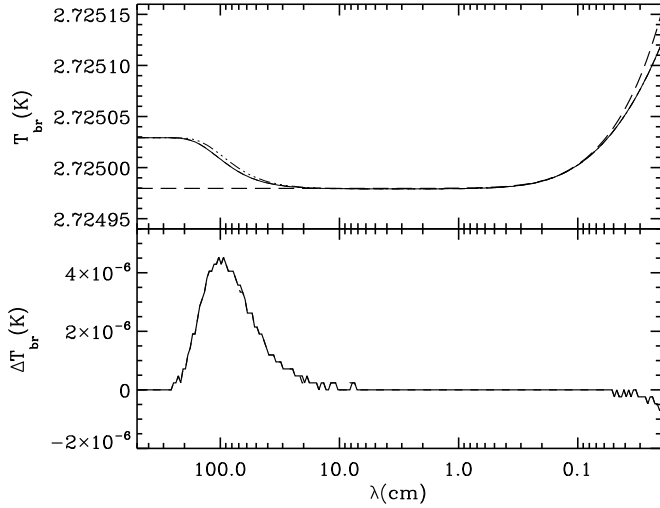


Figure 5. Final (i.e. at $z = 1090$) distorted spectra for different treatments of the recombination process. We assume as initial condition a Comptonization spectrum at $z = 10^4$ characterized by $\Delta\epsilon_r/\epsilon_i = 10^{-5}$. Top panel: initial condition (dashes), final spectrum in the case of instantaneous recombination at $z = 1090$ following the fully ionized phase (three dots-dashes), final spectrum in the case of gradual, more realistic modelizations of the recombination process (the two different treatments give results indistinguishable in these plots). Bottom panel: difference between the final solution found in the case of instantaneous recombination and of gradual, more modelizations. See the text for further details.

While an extensive discussion of various possible applications of these new features of the code, object of future work, is not the scope of this paper, we report here few representative examples.

In Fig. 5 we show the effect of different treatments of the computation of the hydrogen and helium ionization fractions during the recombination epoch in the case of a relatively late spectral distortion. Three different treatments of the recombination history are exploited: an instantaneous recombination following the fully ionized phase and two gradual, more realistic modelizations of the recombination process characterized by different evolutions of ionization fractions. In one of these two cases only the evolution of the electron ionization fraction, χ_e , is taken from the code RECFAST while the H and He ionization fractions are computed solving the system of Saha equations; in the other case we directly use the complete output of the code RECFAST (see Sect. 4.3 and the caption of Fig. 5 for more details). The results obtained in these two cases are identical in practice, while the assumption of full ionization up to $z = 1090$ in the instantaneous recombination case produces a certain overestimate ($\sim 10\%$) of the long wavelength excess due to (essentially free-free) photon production as well as a small amplification ($\sim 1\%$) of the relaxation of the initial Comptonization spectrum towards a Bose-Einstein like spectrum (obviously inefficient, at the considered redshifts). With the adopted numer-

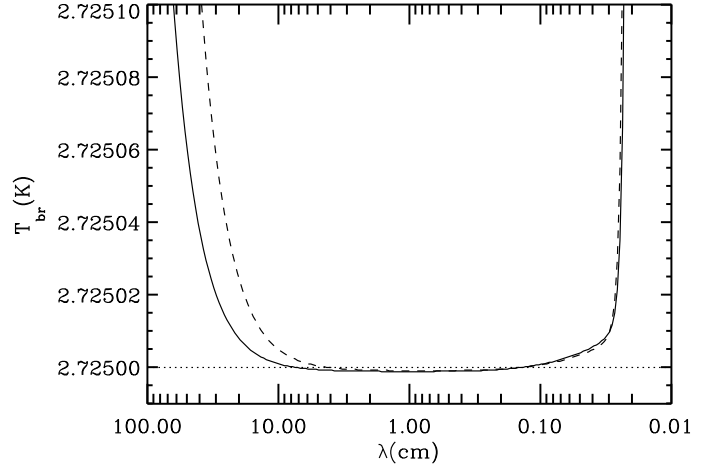


Figure 6. Distorted spectra predicted for the considered reionization models: initial blackbody spectrum (dots) at $z = 20$, almost corresponding to the beginning of the heating phase in the considered model, final (at $z = 0$) spectrum in the case of constant ϕ ($=147$) (dashes) and for the realistic implementation of the ionization and thermal history in the *suppression* model (solid line). See the text for further details.

ical accuracy ($ACC=10^{-12}$) and grid points ($NPTS = 30001$), the required CPU time on the used IBM platform is of about 40 minutes, with less than 20% differences between the three different cases.

Fig. 6 reports the results derived for a particular astrophysical scenario of cosmological reionization. We adopt here the evolution of the electron ionization fraction χ_e (the H and He ionization fractions being then computed solving the system of Saha equations) and of electron temperature predicted in the *suppression* model presented in Schneider et al. (2008) and Burigana et al. (2008) that implies a Thomson optical depth, $\tau \approx 0.1017$, almost in agreement with recent WMAP data (for consistency, we adopt in these computations the same cosmological parameters used in the quoted works). For comparison, we exploit a simple case with full ionization and a constant ratio, ϕ , between the electron temperature and the radiation temperature which is chosen to have the same amount of energy injected in the plasma ($\Delta\epsilon_r/\epsilon_i \approx 7.6 \times 10^{-7}$) obtained in the above realistic model. As expected by construction, the two very different histories produce the same high frequency (Comptonization like) distortion but the long wavelength region is very different because of the contribution of free-free emission¹⁴. The difference of this term in the two cases is mainly characterized by the evolution of the product $\phi^{-1/2}\chi_e^2$ and by the fact that free-free is more efficient at higher redshifts in the simple case than in the realistic one (see the caption of Fig. 6 for more details). With the adopted numerical accuracy ($ACC=10^{-12}$) and grid points ($NPTS = 30001$), the required CPU time on the used IBM platform is of few hours

¹⁴ In both cases, the density contrast in the intergalactic medium associated to the formation of cosmic structures has been not included. The excess at low frequencies due to the free-free distortion should be then considered as lower limit in both cases, since the computation has been performed in the “averaged density” approximation. Therefore, a correction factor $\approx \langle n_e^2 \rangle / \langle n_e \rangle^2 > 1$, coming from a proper inclusion of the treatment of density contrast in the intergalactic medium, should be applied to the free-free term.

for the realistic model and about one hour in the simple model with a constant ϕ .

Finally, we have focussed on some properties of the free-free distortions, relevant for the long wavelength region of the CMB spectrum, by checking that the new code version, as the original one, very accurately recovers the existing analytical approximations in their limit of validity. We have also discussed the relevance of accurate computations able to improve the simple treatment based on the approximation with a frequency independent free-free distortion parameter.

All the tests done demonstrates the reliability and versatility of the new code version and its very good accuracy and applicability to the scientific analysis of current CMB spectrum data and of those, much more precise, that will be available in the future.

7. Acknowledgments

It is a pleasure to thank L. Danese, G. De Zotti, R. Salvaterra, and A. Zizzo for useful discussions and collaborations. Some of the calculations presented here have been carried out on an alpha digital unix machine at the IFP/CNR in Milano and at the IBM SP5/512 machine at CINECA-Bologna by using some NAG integration codes. We warmly thank M. Genghini and C. Gheller for their kind assistance and technical support related to the machines used. We acknowledge the use of the code RECFAST. We acknowledge the support by the ASI contract I/016/07/0 “COFIS”. We thank the anonymous Referee for constructive comments.

References

- Berzins, M. 1990, in *Scientific Software Systems*, eds. J.C. Mason & M.G. Cox, 59, Chapman and Hall, p. 59
- Berzins, M., Dew, P.M., Furzeland, R.M. 1989, *Appl. Numer. Math.*, 5, 375
- Burigana, C., Danese, L., & de Zotti, G. 1991, *A&A*, 246, 49
- Burigana, C., Danese, L., & de Zotti, G. 1991, *ApJ*, 379, 1
- Burigana, C., de Zotti, G., & Danese, L. 1995, *A&A*, 303, 323
- Burigana, C., & Salvaterra, R. 2003, *MNRAS*, 342, 543
- Burigana, C., Salvaterra, R., & Zizzo, A. 2004, *Plasmas in the Laboratory and in the Universe: New Insights and New Challenges*, 703, 397
- Burigana, C., Valenziano, L., De Rosa, A., Salvaterra, R., Procopio, P., Morgante, G., Villa, F., Mandolesi, N. 2007, *Perspectives for Future Experiments and Studies on Cosmic Background Radiation from the Moon*. ASI Contract I/032/06/04, p. 125
- Burigana, C., Popa, L. A., Salvaterra, R., Schneider, R., Choudhury, T. R., & Ferrara, A. 2008, *MNRAS*, 385, 404
- Chang J. S. & Cooper G. 1970, *J. Comput. Phys.*, 6, 1
- Danese L. & Burigana C. 1993, in *Present and Future of the Cosmic Microwave Background*, Lecture in Physics, Vol. 429, eds. J. L. Sanz, E. Martinez-Gonzales, L. Cayon, Springer Verlag, Heidelberg (FRG), p. 28
- Danese, L., & de Zotti, G. 1977, *Rivista del Nuovo Cimento Serie*, 7, 277
- Danese, L., & de Zotti, G. 1980, *A&A*, 84, 364
- Dew, P.M., & Walsh, J. 1981, *ACM Trans. Math. Software*, 7, 295
- de Zotti, G. 1986, *Progress in Particle and Nuclear Physics*, 17, 117
- Fixsen, D. J., Cheng, E. S., Gales, J. M., Mather, J. C., Shafer, R. A., & Wright, E. L. 1996, *ApJ*, 473, 576
- Fixsen, D. J., & Mather, J. C. 2002, *ApJ*, 581, 817
- Gould, R. J. 1984, *ApJ*, 285, 275
- Karzas, W. J., & Latter, R. 1961, *ApJS*, 6, 167
- Kogut, A. 1996, arXiv:astro-ph/9607100
- Kompaneets, A. S. 1956, *Zh. Eksp. Teor. Fiz.*, 31, 876 [*Sov. Phys. JEPT*, 4, 730, (1957)]
- Mather, J. C. 2009, in *Questions of Modern Cosmology – Galileo’s Legacy*, eds. M. D’Onofrio & C. Burigana, Springer, Sect. 5.3.1, p. 435
- Mitchell A.R., Griffiths D.F. 1980, *The Finite Difference Method in Partial Differential Equations*, Wiley, Chichester, U.K.
- The Numerical Algorithms Group Ltd, (2009), Oxford, UK
- Nolta, M. R., et al. 2009, *ApJS*, 180, 296
- Perlmutter, S., et al. 1999, *ApJ*, 517, 565
- Peyraud, N. 1968, *Physics Letters A*, 27, 410
- The Planck Collaboration 2006, *The Scientific Programme of Planck*, ESA-SCI(2005)1, arXiv:astro-ph/0604069
- Press W.H., Flannery B.P., Teukolski S.A., Vetterling W.T., 1992, *Numerical Recipes*, Cambridge University Press
- Riess, A. G., et al. 1998, *AJ*, 116, 1009
- Rybicki G. B., Lightman A. P. 1979, *Radiative processes in astrophysics*, Wiley, New York
- Salvaterra, R., & Burigana, C. 2002, arXiv:astro-ph/0206350
- Salvaterra, R., & Burigana, C. 2002, *MNRAS*, 336, 592
- Schneider, R., Salvaterra, R., Choudhury, T. R., Ferrara, A., Burigana, C., & Popa, L. A. 2008, *MNRAS*, 384, 1525
- Seager, S., Sasselov, D. D., & Scott, D. 1999, *ApJ*, 523, L1
- Silk, J., & Stebbins, A. 1983, *ApJ*, 269, 1
- Singal, J., et al. 2009, arXiv:0901.0546
- Skeel, R.D., & Berzins, M. 1990, *SIAM J. Sci. Statist. Comput.*, 11(1), 1
- Sunyaev, R. A., & Zeldovich, Y. B. 1970, *Ap&SS*, 7, 20
- Tricomi F. G. 1957, *Equazioni a Derivate Parziali*, ed. Cremonese, Roma
- Wong, W. Y., Moss, A., & Scott, D. 2008, *MNRAS*, 386, 1023
- Zannoni, M., Tartari, A., Gervasi, M., Boella, G., Sironi, G., De Lucia, A., Passerini, A., & Cavaliere, F. 2008, *ApJ*, 688, 12
- Zeldovich Ya.B., Illarionov A.F., Sunyaev R.A. 1972, *Zh. Eksp. Teor. Fiz.*, 62, 1216 [*Sov. Phys. JEPT*, 35, 643]
- Zeldovich, Y. B., & Levich, E. V. 1970, *Zh. Eksp. Teor. Fiz.*, 11, 57
- Zeldovich Ya.B., Sunyaev R.A. 1969, *Ap&SS*, 4, 301
- Zizzo, A., & Burigana, C. 2005, *New Astronomy*, 11, 1